
Simpler Fast Vision Transformers with a Jumbo CLS Token

Anthony Fuller¹ Yousef Yassin¹ Daniel G. Kyrollos¹ Evan Shelhamer^{2,3} James R. Green¹

Abstract

We introduce a simple enhancement to the global processing of vision transformers (ViTs) to improve accuracy while maintaining throughput. Our approach, Jumbo, creates a wider CLS token, which is split to match the patch token width before attention, processed with self-attention, and reassembled. After attention, Jumbo applies a dedicated, wider FFN to this token. Jumbo *significantly* improves over ViT+Registers (Darcet et al., 2024) on ImageNet-1K at high speeds (by 3.2% for ViT-tiny and 13.5% for ViT-nano); these Jumbo models even outperform specialized compute-efficient models while preserving the architectural advantages of plain ViTs. Although Jumbo sees no gains for ViT-small on ImageNet-1K, it gains 3.4% on ImageNet-21K over ViT+Registers. Both findings indicate that Jumbo is most helpful when the ViT is otherwise too narrow for the task. Finally, we show that Jumbo can be easily adapted to excel on data beyond images, e.g., time series.

1. Introduction

There has been tremendous progress in computer vision over the past decade. Innovations have resulted in models with greater absolute accuracy, greater speed for a given accuracy, and greater simplicity. Vision transformers (ViTs) (Dosovitskiy et al., 2021) exemplify this progress.

ViTs are *simple*. They split an image into patches, linearly project patches to form patch embeddings, add position embeddings to patch embeddings, prepend a learnable “CLS” token, and then process this set of vectors with a transformer; these operations can be implemented in a single file of ~ 100 lines of PyTorch (Paszke et al., 2019)¹. ViTs are *flexible*. They offer seamless sparse computation via token

¹Carleton University, Ottawa, Canada. ²University of British Columbia, Vancouver, Canada. ³Vector Institute. Correspondence to: Anthony Fuller <anthonyfuller@cmail.carleton.ca>.

Preprint.

¹For example: https://github.com/lucidrains/vit-pytorch/blob/main/vit_pytorch/vit.py

dropping (He et al., 2022; Akbari et al., 2021; Liu et al., 2023b), patch resizing (Beyer et al., 2023; Liu et al., 2024), image size extrapolating (Fuller et al., 2024), model scaling (Zhai et al., 2022; Dehghani et al., 2023), and multimodal processing (Dou et al., 2022; Xu et al., 2023). ViTs are *effective*. They achieve state-of-the-art (SOTA) performance in image classification (Touvron et al., 2022; Alabdulmohsin et al., 2024), object detection (Li et al., 2022a; Liu et al., 2025), and semantic segmentation (Li et al., 2024b); ViTs are core components of vision-language models (Bai et al., 2023; Liu et al., 2023a). However, plain ViTs often underperform more specialized architectures w.r.t. compute efficiency, especially at high speeds.

Many recent architectures improve the computational efficiency of ViTs (Cai et al., 2023; Mehta & Rastegari, 2021; Vasu et al., 2023b; Yun & Ro, 2024), where an improvement in efficiency typically refers to achieving a better accuracy-speed trade-off. These architectures leverage a *hierarchical* design, following classic architectures, such as ResNets (He et al., 2016) and VGGNets (Simonyan, 2014) — they progressively reduce spatial dimensions while increasing channel width. A larger width corresponds to a larger feed-forward network (FFN), which increases model capacity by enabling non-linear processing over more dimensions. Yet, the *cost* of larger FFNs is controlled in these architectures by decreasing the number of patches/tokens. We highlight this added capacity at little computational cost as a common element of such models. These efficient architectures typically intersperse modules such as convolutions, pooling, sparse or linear attention, and other innovations with standard ViT modules (i.e., self-attention and point-wise FFNs). However, these innovations eliminate the desirable properties of plain ViTs we wish to keep, such as token dropping and multimodal support.

Increasing the depth and/or width is the standard approach to increase ViT model capacity (Zhai et al., 2022). Recently Darcet et al. (2024) increase the number of parameters by adding learnable tokens called “registers”. Registers scale capacity asymmetrically by adding global capacity (= inter-token modeling) without adding local capacity (intra-token modeling). This addresses a key weakness in ViTs that they identify: *plain ViTs have insufficient global capacity*. They show that adding registers improves the classification and segmentation performance of plain ViTs. However,

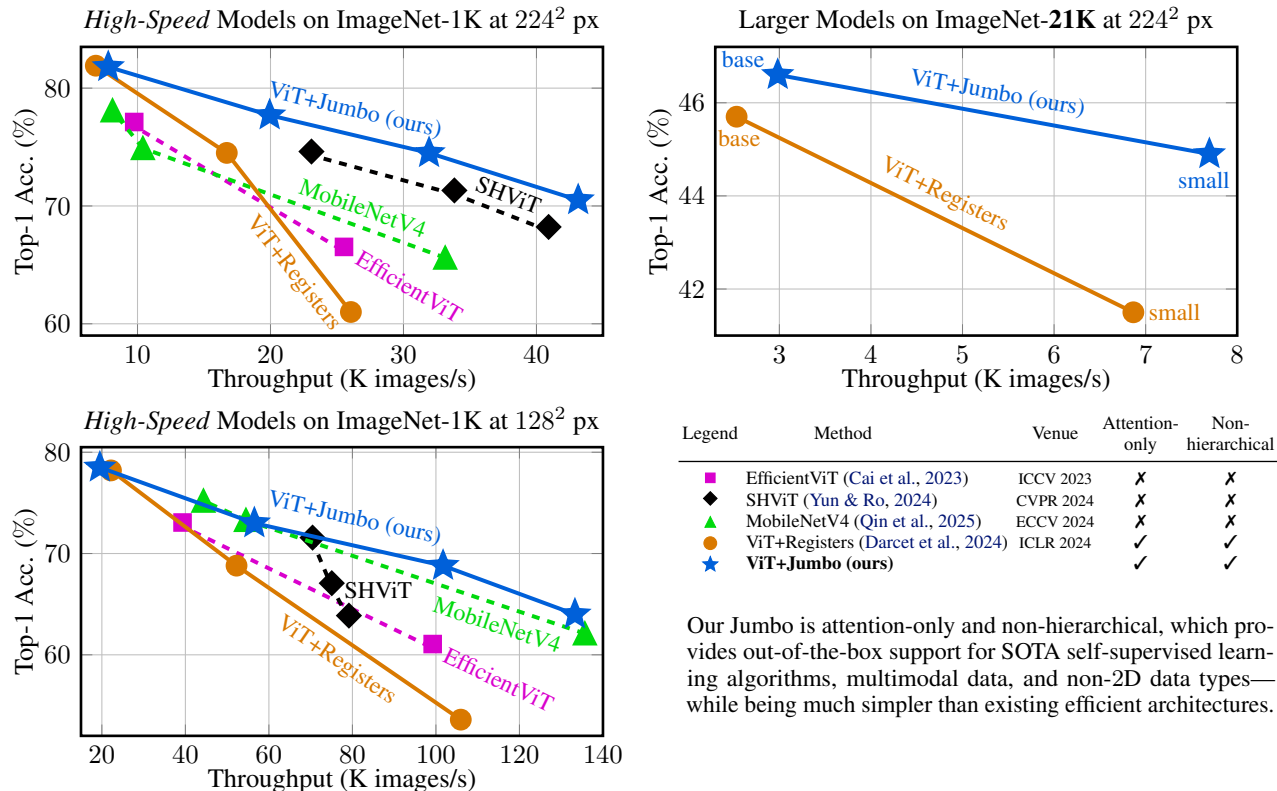


Figure 1. ViT+Jumbo outperforms SOTA compute-efficient architectures while preserving the advantages of plain ViTs. ViT+Jumbo equals or outperforms ViT+Registers on the standard ImageNet-1K and strictly improves on the challenging ImageNet-21K dataset. Throughput is measured on an RTX 4090 GPU using PyTorch 2.6.0, `torch.compile`, and a 512 batch size.

the global information in registers only interacts through attention (i.e., a weighted sum of linear projections). This limits the ability of ViT+Registers to learn more complex functions of global features, which we address here.

Our method, called Jumbo, increases the width of the CLS token to J times the patch width. Before self-attention, our method splits this extra wide Jumbo token into J smaller tokens, includes them in self-attention, and then concatenates them to reassemble a single Jumbo token. Rather than sharing FFN parameters with all patches, Jumbo leverages a wider CLS-specific FFN to increase model capacity. The cost of this larger FFN is minimal because it only processes a single token. Crucially, Jumbo preserves all the advantages of plain ViTs previously discussed, while efficiently adding global capacity. This includes support for token dropping, which is critical for many self-supervised learning (SSL) algorithms (Wei et al., 2025; Assran et al., 2023; He et al., 2022; Fu et al., 2024).

We show that ViT+Jumbo significantly outperforms ViT+Registers in three scenarios through apples-to-apples comparisons. Specifically, Jumbo clearly improves in image classification: ① on ImageNet-1k at ViT-tiny and ViT-nano sizes, and ② on ImageNet-21k at sizes up to ViT-base. These results lead to an insight: Jumbo helps most when the ViT

is otherwise too narrow for the task.

In fact, ViT+Jumbo at tiny and nano scales outperforms specialized compute-efficient architectures, such as EfficientViT (Cai et al., 2023). To our knowledge, ViT+Jumbo is the first attention-only and non-hierarchical architecture to even be competitive with compute-efficient architectures at high speeds. These two properties make ViT+Jumbo compatible out-of-the-box with SOTA SSL and adaptable to other data modalities such as time series.

③ As an example of applying Jumbo beyond vision, we show that the simple incorporation of Jumbo for time series tasks improves performance over PatchTST (Nie et al., 2023) and PatchTST+Registers.

2. Background and Related Work

2.1. Vision Transformers

A ViT splits an image into a grid of non-overlapping patches, $\mathbb{R}^{Y \times X \times C} \rightarrow \mathbb{R}^{N_y \times N_x \times P_y \times P_x \times C}$, where C is the number of channels, Y/X are the image height/width, N_y/N_x are the grid height/width, and P_y/P_x are the patch height/width in pixels (equal to $\frac{Y}{N_y} / \frac{X}{N_x}$). Next, they flatten the grid into a sequence and flatten the patches into vectors,

$\mathbb{R}^{N_y \times N_x \times P_y \times P_x \times C} \rightarrow \mathbb{R}^{N \times D_{pix}}$, where N is the number of patches (equal to $N_y \cdot N_x$), and D_{pix} is the number of pixel values per patch (equal to $P_y \cdot P_x \cdot C$). Next, they apply a learnable linear projection to form patch embeddings, $\mathbb{R}^{N \times D_{pix}} \rightarrow \mathbb{R}^{N \times D}$, where D is the model width, also known as the embedding dimension. Next, they add position embeddings to patch embeddings. (Superior and slightly more complex position encoding methods exist (Weinzaepfel et al., 2023; Heo et al., 2025; Fuller et al., 2024); however, we simply use learnable embeddings in this work — although Jumbo is also compatible with all these other methods.) These operations produce local tokens $\mathbf{x}^P \in \mathbb{R}^{N \times D}$ that represent *highly* local information — typically a 16×16 px square. Crucially for this work, ViTs prepend a learnable CLS token \mathbf{x}^{CLS} to the sequence of local tokens, $\mathbf{x} = \mathbf{x}^{CLS} \parallel_0 \mathbf{x}^P \in \mathbb{R}^{(N+1) \times D}$, where \parallel_0 denotes concatenation along the 0th (sequence) dimension. Finally, the input \mathbf{x} is processed by a plain transformer and the — now contextualized — CLS token can be used for image classification.

Sizes. ViT sizes vary w.r.t. depth and width. The models we train all have 12 layers, while the widths vary $\{96, 128, 192, 384, 768\}$, corresponding to names $\{\text{pico, nano, tiny, small, base}\}$. We name pico and nano sizes inspired by Woo et al. (2023).

A standard image size of 224×224 px and a standard patch size of 16×16 px results in 196 local tokens. A *single* CLS token — that is designed to aggregate global information to facilitate classification — provisions $1/197^{\text{th}}$ of a model’s representational capacity to global information (and this fraction decreases with larger images and/or smaller patches). This allocation seems suboptimal. Recent work finds evidence to support this intuition and proposes a fix.

Registers. Darcet et al. (2024) find that ViTs are so hungry for more CLS tokens that they *learn* to repurpose some local patch tokens into “pseudo-CLS” tokens; these co-opted tokens behave like CLS tokens — they aggregate global information and discard patch-specific local information. Darcet et al. (2024) propose a fix: prepend additional learnable tokens — called registers $\mathbf{x}^{\text{Reg}} \in \mathbb{R}^{R \times D}$, where R is the number of registers — to the input sequence, $\mathbf{x} = \mathbf{x}^{CLS} \parallel_0 \mathbf{x}^{\text{Reg}} \parallel_0 \mathbf{x}^P \in \mathbb{R}^{(N+R+1) \times D}$. Registers improve performance and reduce attention map artifacts by provisioning more global capacity.

Adding registers is elegantly simple to implement, and they preserve the advantages of plain ViTs; they can natively drop tokens and are compatible with SOTA self-supervised learning algorithms. In theory, registers can benefit any plain, noncausal transformer. These several advantages account for registers’ *significant and immediate* impact, including their application beyond image data (Dong et al., 2024; Vaquero et al., 2024; Leigh et al., 2024; Messaoud

et al., 2025; Hu et al., 2024; Thimonier et al., 2024; Omranpour et al., 2024). For these reasons, ViT+Registers is the primary inspiration behind our method, Jumbo.

Hiera. Our work aligns spiritually with Hiera (Ryali et al., 2023), simplifying hierarchical transformers, such as Swin (Liu et al., 2021) or MViT (Fan et al., 2021), by replacing convolutions with pooling layers. Although hierarchical models are incompatible with token dropping out-of-the-box, Ryali et al. (2023) engineer a solution allowing Hiera to be pretrained with masked autoencoding (He et al., 2022). However, Hiera is not fast — e.g., its fastest variant has $0.58\times$ the throughput of our Jumbo ViT-small.

2.2. Compute Efficient Architectures

We highlight 3 architectures and use them as baselines for a high-speed ViT. ❶ EfficientViT (Cai et al., 2023) and ❷ SHViT (Yun & Ro, 2024) improve the efficiency of ViTs by incorporating efficient attention, pooling, and convolutional layers. ❸ MobileNetV4 (Qin et al., 2025) improves the efficiency of CNNs by leveraging many strategies (and different strategies for different model sizes). These baselines represent the SOTA in computational efficiency; please refer to Appendix A.1 for descriptions of these model architectures.

Beyond these, there is a rich literature on compute-efficient computer vision architectures. For example, several efficient CNN-based architectures exist (Howard, 2017; Sandler et al., 2018; Howard et al., 2019; Han et al., 2020; Tan et al., 2019; Vasu et al., 2023a); however, these have been recently surpassed by MobileNetV4 (Qin et al., 2025). Since the invention of the ViT (Dosovitskiy et al., 2021), there have been many compute-efficient “ViTs” that incorporate efficient modules inspired by CNN-based approaches (Vasu et al., 2023b; Mehta & Rastegari, 2021; 2022; Li et al., 2023; Pan et al., 2022; Chen et al., 2022; Li et al., 2022b). SHViT (Yun & Ro, 2024) has recently surpassed these architectures. Despite their impact and ingenuity, none of these hybrid architectures meets the definition of a plain ViT, which is attention-only and non-hierarchical; they thus lose many advantages of ViTs that we wish to keep.

3. Method

3.1. Design Motivation and Intuition

Capacity. Registers increase the global capacity of plain ViTs. Registers “communicate” with each other through attention. And attention is best thought of as a mechanism that *moves* information between tokens (Elhage et al., 2021). While the attention sublayer is a crucial component of transformers, its expressive capacity, alone, is inherently limited. Conversely, an FFN (equivalent to an MLP with 1 hidden layer) accepts a single token as input, and processes this information by applying a learned non-linear function. By

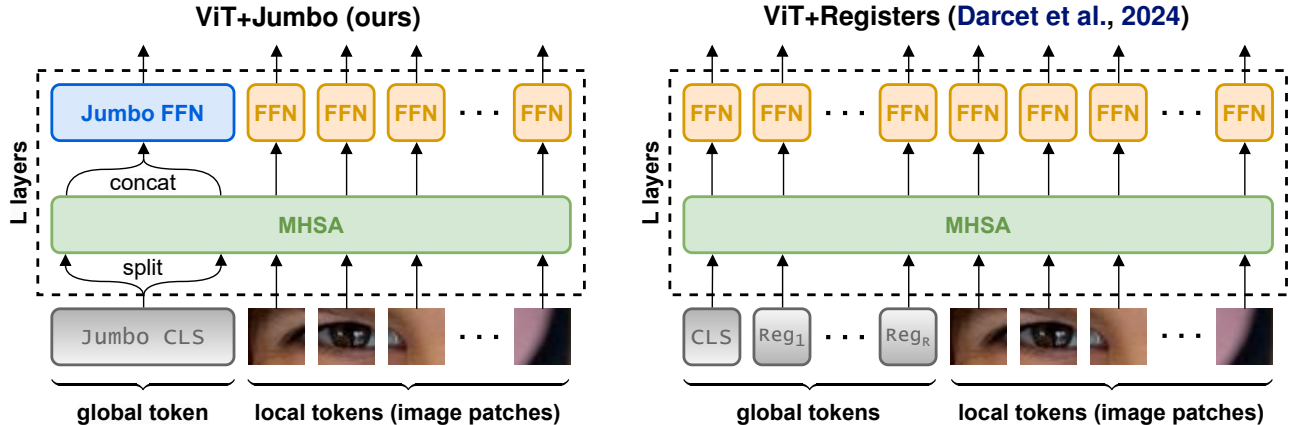


Figure 2. (Left) Our ViT+Jumbo method creates a wider CLS token that gets split into several tokens, with width equal to the patch width, prior to multi-headed self-attention (MHSA). After attention, the split Jumbo CLS token is reassembled via concatenation, and is then processed by *its own* FFN. Patches are processed by *their own, shared* FFN. (Right) ViT+Registers creates many register tokens all equal to the patch width. All registers, patches, and the CLS token are processed by a *shared* FFN. ViT+Jumbo enhances global processing as the (split) global tokens can interact via an FFN, in addition to attention.

concatenating our global tokens (i.e., the split Jumbo token) and sending the resultant Jumbo token through an FFN, we can model more complex functions of global features.

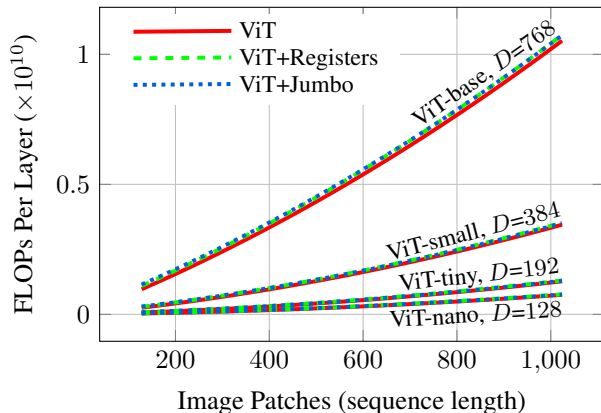


Figure 3. The cost of a ViT layer is—almost entirely—determined by the number of image patches and the patch width D . The cost of adding registers ($R = 16$) or our Jumbo CLS token ($J = 6$) is negligible.

Cost. Although Jumbo adds global capacity, its cost is minimal. The key insight is that the larger FFNs only process a single token. As shown in Fig. 3, the primary drivers of computational cost (FLOPs per layer) are sequence length and patch width, D . The FLOP contribution from adding registers or our Jumbo token is comparatively negligible. We discuss Jumbo’s parameter increase in Section 5.

Non-hierarchical and attention-only. Jumbo preserves the non-hierarchical (sometimes called columnar or isotropic) shape of ViTs and ViT+Registers. And, by foregoing con-

volutions, spatial information only moves through attention. These features have several advantages that we now discuss.

❶ Attention-only models can efficiently **drop tokens**. Although convolutions are capable of processing a sparse subset of patches via sparse compute kernels, these kernels can be complex, challenging to use, and require updating when new hardware arrives. Furthermore, sparse convolutional kernels will never be as efficient as simply indexing from a sequence — i.e., how transformers drop tokens. As one point of comparison, ConvNeXt V2 (Woo et al., 2023) reports a $1.3\times$ speedup using a 60% masking ratio with the Minkowski Engine v0.5.4 (Choy et al., 2019). Conversely, MAE (He et al., 2022) report $2.8 - 4.1\times$ speedups using a 75% masking ratio with plain ViTs. Efficient token dropping is required for most SOTA SSL algorithms, for example, I-JEPA (Assran et al., 2023), CrossMAE (Fu et al., 2024), Image World Models (Garrido et al., 2024), LatentMIM (Wei et al., 2025), etc. Token dropping is also used to speedup plain supervised training (Dehghani et al., 2024); we demonstrate this use of token dropping in subsection 4.2.

❷ Non-hierarchical and attention-only models can be easily adapted to **other data modalities**. For example, 1D time series, 3D point clouds, or multimodal data; users need only adjust tokenization strategies. We demonstrate a 1D time series application of Jumbo in subsection 4.3.

❸ Non-hierarchical and attention-only models can more easily benefit from other deep learning advances; i.e., they can **“piggyback” off other innovations**. ❶ Many recent SSL methods are designed for the plain ViT’s non-hierarchical shape (Wei et al., 2025; Assran et al., 2023; Garrido et al., 2024). ❷ Many recent segmentation and object detection “heads” are designed for the plain ViT’s non-hierarchical

shape (Fang et al., 2023; Liu et al., 2025; Zhang et al., 2022).

❶ Many recent advances in compute kernels for plain self-attention decrease its cost. For example, Flash Attention (Dao et al., 2022; Dao, 2023; Shah et al., 2024) can speed up self-attention by more than $5\times$. Jumbo immediately benefits from these advances.

Conversely, *none* of the compute-efficient architectures cited in subsection 2.2 immediately benefit from these advances. None of them support other data modalities. And none of them support token dropping.

Two hypotheses. Jumbo asymmetrically increases the network width. Thus, ❶ we expect increasing gains due to Jumbo with *decreasing* patch token width. In other words, the more width-deprived a network, the more Jumbo should help. However, what it means to be “width-deprived” is not straightforward. Intuitively, tasks requiring reasoning over *more concepts* must require *more width* to store these concepts and facilitate reasoning over them. Thus, ❷ we expect increasing gains due to Jumbo with *increasing* task output dimensionality. We explore both of these hypotheses using experiments with ViTs of different widths and datasets of different complexities.

3.2. Design Specifics

Exactly like the original ViT, Jumbo computes patch embeddings, $\mathbf{x}^P \in \mathbb{R}^{N \times D}$. Unlike the original ViT, our method creates a Jumbo CLS token that is J times wider than the patch width D , $\mathbf{x}^{\text{Jumbo}} \in \mathbb{R}^{J \cdot D}$. Architecturally identical transformer layers then process these inputs.

Before self-attention, the Jumbo token is split into J tokens, $\big|_J^1 \mathbf{x}^{\text{Jumbo}} : \mathbb{R}^{1 \times J \cdot D} \rightarrow \mathbb{R}^{J \times D}$, where $\big|_J^1$ denotes splitting into J segments along the 1st (feature) dimension. Next, the split Jumbo token is concatenated with patch embeddings along the sequence dimension, $\mathbf{x} = \mathbf{x}^{\text{Jumbo}} \parallel_0 \mathbf{x}^P \in \mathbb{R}^{(N+J) \times D}$. This sequence is sent through a plain multi-headed self-attention layer. Afterward, the Jumbo token is extracted from the sequence by splitting along the sequence dimension, $\big|_2^0 \mathbf{x} : \mathbb{R}^{(N+J) \times D} \rightarrow (\mathbb{R}^{J \times D}, \mathbb{R}^{N \times D})$, where the first element contains the (still split) Jumbo token and the second element contains the patch representations. Finally, the Jumbo token is reassembled through concatenation along the channel dimension, $\mathbf{x}^{\text{Jumbo}} = \big|_1 \mathbf{x}^{\text{Jumbo}} : \mathbb{R}^{J \times D} \rightarrow \mathbb{R}^{1 \times J \cdot D}$. These two splits and two concatenations add negligible runtime overhead.

After self-attention, the Jumbo token is processed by its own FFN; i.e., it does not share parameters with the patch-wise FFN. We indicate this in Fig. 2 by coloring Jumbo and patch-wise FFNs differently. After all layers process the image, our method projects the Jumbo token to C class logits, $\mathbb{R}^{J \cdot D} \rightarrow \mathbb{R}^C$. Since the patch-wise FFNs in the last layer are unused, we discard them.

4. Experiments

For all experiments, we measure throughput on an RTX 4090 GPU using PyTorch 2.6.0, `torch.compile`, and a 512 batch size.

4.1. High-Speed Experiments

We take a different experimental approach to many prior works. Typically, these works train models with their novel architecture on ImageNet-1K for 300 epochs. They perform (often extensive) tuning and directly compare with results reported by baselines. For example, MobileNetV4 (Qin et al., 2025) tunes the architecture for each model scale (small, medium, etc.) using neural architecture search (NAS). Furthermore, each model scale is often trained with a different hyperparameter “recipe” — in the case of MobileNetV4 each recipe comprises 10+ hyperparameters that seem tuned. This methodology results in *highly* valuable artifacts — i.e., trained model weights — that practitioners can download and use.

However, this approach makes building atop such research challenging, as the relative contributions between architecture and training recipe can be unclear. Furthermore, the robustness of the results w.r.t. the training recipe can also be unclear, leading to significant uncertainty when leveraging the novel architecture in different settings.

Informed by these observations, we perform apples-to-apples comparisons, which includes training SOTA high-speed models ourselves.

4.1.1. EXPERIMENTAL DETAILS

Setup. We train models from scratch on ImageNet-1K (Rusakovsky et al., 2015) using function matching (Beyer et al., 2022) with a highly accurate teacher (85.7% top-1 accuracy on ImageNet-1K (Touvron et al., 2022)) at 128×128 px for 400 epochs. Then we finetune each model at 224×224 px for 20 epochs with a more accurate (but expensive) teacher (87.0% top-1 accuracy on ImageNet-1K (Touvron et al., 2022)). Each run takes 4-5 days on an RTX 4090 GPU.

This approach has three advantages. ❶ By training at two resolutions, we can compare the accuracy-speed trade-offs of models at two resolutions (rather than a single comparison point). ❷ By training at a lower resolution for the majority of epochs, we save *significant* training cost, and models benefit from the FixRes effect (Touvron et al., 2019; 2022). ❸ By leveraging a SOTA distillation method, models benefit from greater sample efficiency. Importantly, both low-res to high-res training and function matching are *architecture agnostic* — they were invented with CNNs and are used with ViTs.

We train each model architecture twice, once for each learn-

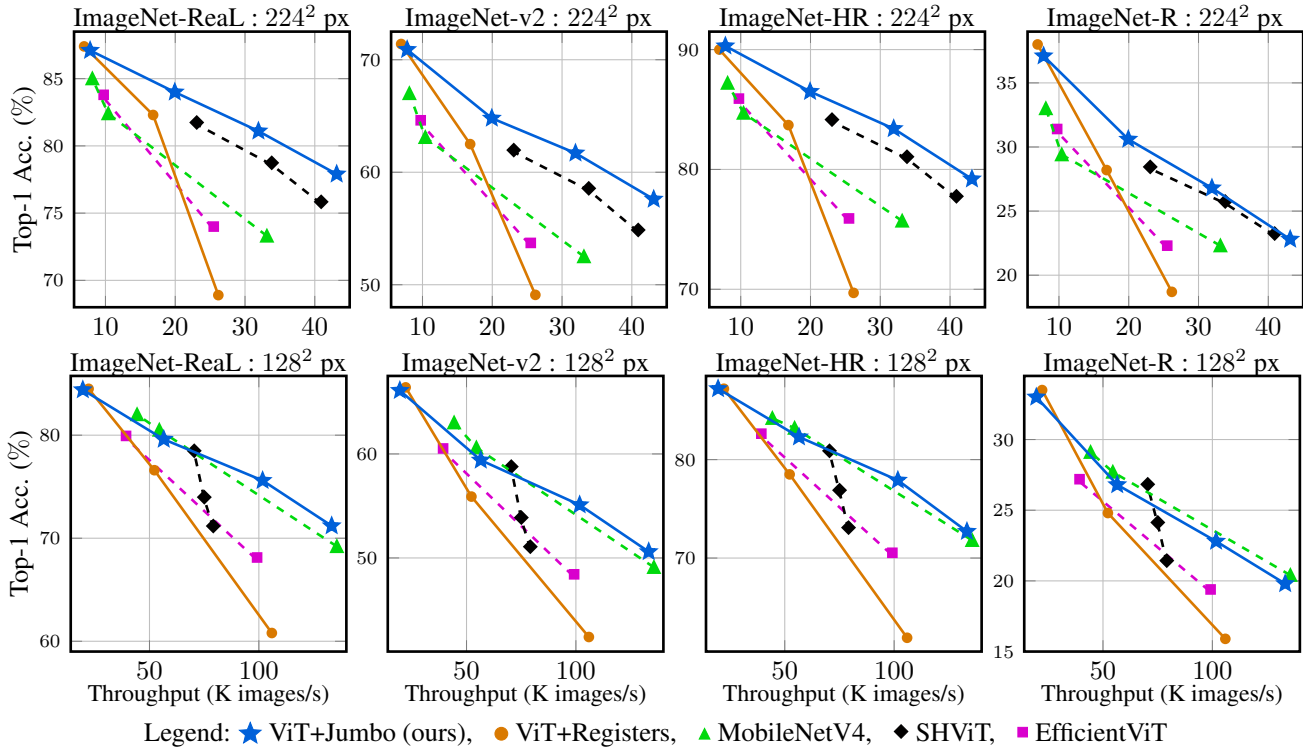


Figure 4. ViT+Jumbo mostly achieves the Pareto frontier, while being much simpler than specialized compute-efficient model architectures. Results from each model’s best learning rate is plotted. Throughput is measured on an RTX 4090 GPU using PyTorch 2.6.0, `torch.compile`, and a 512 batch size.

ing rate $\{1e-3, 3e-3\}$ using a 1024 batch size with the AdamW optimizer (Loshchilov, 2017). We report the results of the best learning rate for each model architecture. Please see Appendix A.2.1 for the complete results and hyperparameters.

Baselines. We choose the fastest models for each family: ① ViT+Registers {nano, tiny, small} (Darcet et al., 2024), ② EfficientViT {B0, B1} (Cai et al., 2023), ③ SHViT {S1, S2, S3} (Yun & Ro, 2024), and ④ MobileNetV4 {conv-small, conv-medium, hybrid-medium} (Qin et al., 2025). We compare these architectures with our fastest ViT+Jumbo variants {pico, nano, tiny, small}. Darcet et al. (2024) show ViT+Registers with $R=16$ performs best, which we confirm in Appendix A.2.3 and use in these experiments. We show ViT+Jumbo is robust to the choice of J ; we use $J=6$ and study its effect in subsection 4.4.

Test Sets. We test all models on the three most common ImageNet-1K test sets: ImageNet-Val (Russakovsky et al., 2015), ImageNet-RealL (Beyer et al., 2020), and ImageNet-v2 (Recht et al., 2019). We also test all models on a newer, high-quality ImageNet-1K test set, ImageNet-HR (Fuller et al., 2024), and an out-of-distribution test set, ImageNet-R (Hendrycks et al., 2021).

4.1.2. HIGH-SPEED RESULTS

As illustrated in Fig 4, Jumbo mostly achieves the Pareto frontier among fast models on ImageNet-1K. We highlight the significance of these results, as Jumbo achieves them while preserving the many advantages and simplicity of plain ViTs; even matching the specialized compute-efficient architectures makes a strong case for ViT+Jumbo.

ViT+Jumbo outperforms ViT+Registers by 13.5% at the nano scale and 3.2% at the tiny scale, tested on 224×224 px images. These are *significant* gains. And it confirms our first hypothesis that Jumbo’s gains should increase as we decrease the patch width, i.e., from small ($D=384$) to tiny ($D=192$) to nano ($D=128$).

If a researcher or practitioner requires out-of-the-box support for SSL algorithms or multimodal processing, *and* requires a fast model, ViT+Jumbo is a clear choice. ViT+Registers is not performant at high speeds, while the specialized compute-efficient architectures do not support most SOTA SSL algorithms or multimodal processing. Remote sensing (Rolf et al., 2024) and autonomous driving (Muhammad et al., 2020) are two of many applications where this combination of speed, SSL support, and multimodal processing is particularly valuable.

At the ViT-small scale (i.e., depth=12, width=384),

ViT+Jumbo has *no* gains over ViT+Registers — at least on ImageNet-1K. However, there is no fundamental reason to see gains generally stop at the ViT-small scale. It seems like a 384-d CLS token can sufficiently model ImageNet-1K’s output dimensionality. Furthermore, this singular negative result leads us to test our second hypothesis that Jumbo’s gains should increase on tasks that require reasoning over a larger concept space.

4.2. ImageNet-21K Experiments

ImageNet-1K is a subset of the more challenging, original ImageNet (Deng et al., 2009), now commonly referred to as ImageNet-21K. We use a common variant comprising 10450 classes; this is a processed variant intended to make training on ImageNet-21K more accessible (Ridnik et al., 2021) (they call this variant ImageNet-21K-P, but we refer to it as ImageNet-21K). This dataset provides more than $\times 10$ the number of classes and samples as ImageNet-1K — making it well suited to test our second hypothesis.

4.2.1. EXPERIMENTAL DETAILS

Setup. We train models from scratch on ImageNet-21K (Ridnik et al., 2021). Since training models on ImageNet-21K is expensive, we leverage a token dropping strategy to reduce costs. Specifically, we start training with a 90% token drop rate and linearly decrease this value to 10%; this halves the total number of tokens processed. Dehghani et al. (2024) demonstrate the effectiveness of this strategy, i.e., leveraging “masking” with plain supervised training. Moreover, all the models that we train on ImageNet-21K support token dropping with minimal code changes.

We train each model architecture once, for 50 epochs using a $3e-3$ learning rate and a 1024 batch size with the AdamW optimizer (Loshchilov, 2017) (see Appendix A.2.1 for other hyperparameters). Each ViT-base run takes 7 days, and each ViT-small run takes 3.3 days on an RTX 4090 GPU.

Baselines. We choose ViT+Registers {small, base} to compare with our ViT+Jumbo {small, base} sizes. This is a more narrow but valid comparison, as the plain ViT is the vision community’s preferred architecture at these scales — due to its simplicity, flexibility, and out-of-the-box compatibility with SSL algorithms. For ViT+Registers, we use $R=16$; for ViT+Jumbo, we use $J=6$ for the small model (since it worked well on ImageNet-1K) and $J=3$ for the base model (since $J=6$ did not fit in memory; we discuss and demonstrate a solution to this limitation in section 5).

4.2.2. IMAGENET-21K RESULTS

ViT+Jumbo outperforms ViT+Registers by 3.4% and 1.0% at ViT-small and ViT-base scales, respectively (see Fig. 1b). These significant gains confirm our second hypothesis that

Jumbo’s gains should increase with increasing output dimensionality. Since Jumbo scales favorably with output dimensionality, we expect Jumbo to excel at CLIP-like (Radford et al., 2021) vision-language frameworks, where the ViT is tasked with modeling a vocabulary with 50K+ terms. However, these experiments require even more resources, so we save them for future work.

4.3. Time Series Experiments

Users can easily adapt Jumbo to different input shapes, i.e., beyond images. This subsection demonstrates one such adaptation to time series inputs.

PatchTST (Nie et al., 2023) is a SOTA patch-based transformer architecture for time series processing, designed to address the limited semantic meaning carried by individual points in time. We extend PatchTST by introducing registers to its transformer backbone (PatchTST+Registers) and incorporating Jumbo (PatchTST+Jumbo).

4.3.1. EXPERIMENTAL DETAILS

Setup. We train models from scratch on ① 10 univariate time series datasets from the UCR archive (Dau et al., 2018), and ② 10 multivariate time series datasets from the UEA archive (Bagnall et al., 2018); both of which are commonly used benchmarks (Zerveas et al., 2021; Grover et al., 2024; Le et al., 2024). For each dataset and model architecture, we perform a hyperparameter sweep that is the result of the following Cartesian product: learning rate $\{3e-3, 1e-3, 3e-4, 1e-4\}$, and dropout $\{0.0, 0.1, 0.2\}$. Additional hyperparameter and training details are provided in Appendix A.2.2, where we also report both the best run and the average of all 12 runs per dataset and architecture. To summarize these many results, we compute the rank between models, then average the ranks over the 10 univariate and 10 multivariate datasets.

Baselines. We compare PatchTST with our PatchTST+Jumbo models and create PatchTST+Registers as an additional baseline. We experiment with 8 and 42 patches per sequence for all three architectures. Importantly, adding our Jumbo CLS token or registers to the PatchTST architecture is simple to adopt.

4.3.2. TIME SERIES RESULTS

Our extensive evaluations demonstrate that PatchTST+Jumbo outperforms strong PatchTST and PatchTST+Registers baselines (Tab. 1). In particular, Jumbo gains the most with fewer patches and when results are averaged across all runs. These results demonstrate Jumbo’s potential in applications that leverage plain, noncausal transformers. As transformers are increasingly adopted in a wide variety of important science and

Table 1. Time series rankings using the PatchTST framework with Registers or Jumbo (*lower is better* and the best ranking is in bold). We rank over 10 univariate datasets and 10 multivariate datasets. “Best” refers to the best run of our 12-run hyperparameter sweep and “Avg” refers to the average over the sweep. Jumbo achieves the best ranking in all experiments.

(a) PatchTST (Nie et al., 2023) with 8 patches.

		PatchTST/8	PatchTST/8 +Registers	PatchTST/8 +Jumbo
Univariate	Best	2.0	2.5	1.5
	Avg	2.9	2.1	1.0
Multivariate	Best	2.1	2.1	1.6
	Avg	2.7	2.0	1.3

(b) PatchTST (Nie et al., 2023) with 42 patches.

		PatchTST/42	PatchTST/42 +Registers	PatchTST/42 +Jumbo
Univariate	Best	1.9	2.1	1.7
	Avg	2.3	2.4	1.3
Multivariate	Best	2.0	1.9	1.7
	Avg	2.6	2.4	1.0

engineering challenges, improving plain transformers (rather than application-specific niche improvements) will achieve broader impact.

4.4. Ablations

Table 2. Jumbo multiplier J and inner Jumbo FFN multiplier ablations. Throughput measurements and evaluations are performed on 128×128 px images. Our default values are in gray.

Patch Width	Jumbo Multiplier	Inner FFN Multiplier	Throughput imgs/s	ImageNet-Val % Top-1 Acc.
192	2	2	71.6K	70.0
		4	69.6K	70.4
	4	1	69.6K	71.5
		2	68.1K	70.6
	6	4	64.9K	72.2
		1	65.3K	72.1
384	2	2	27.2K	77.0
		4	26.1K	78.1
	4	1	26.1K	77.3
		2	24.5K	77.9
	6	4	23.6K	77.9
		1	23.9K	77.6
	2	22.9K	77.8	
		4	19.5K	78.3

Setup. We follow our ImageNet-1K training recipe, training models using function matching (Beyer et al., 2022), for 400 epochs at 128×128 px. We vary the Jumbo multiplier, J , and the inner Jumbo FFN multiplier; this inner multiplier increases the hidden size of the Jumbo FFN, and we always use the default value of 4 for patches. We test models at 128×128 px.

Table 3. We limit Jumbo’s parameter increase by sharing Jumbo weights across layers. Separately, we let the Jumbo layers differ via layer-specific LoRAs (Hu et al., 2022). Both methods effectively control Jumbo’s parameter increase while maintaining strong performance. We measure throughput/memory on an RTX 4090 GPU with a 512 batch size; we train and test models on ImageNet-21K.

Architecture	Throughput imgs/s	Params M	Memory GB	Top-1 Acc. %
ViT+Registers, $R=16$	8.4K	25.7	3.47	41.48
ViT+Jumbo, $J=6$	8.0K	555.6	5.39	44.95
ViT+Jumbo, layer share, $J=6$	8.2K	88.3	3.76	44.61
ViT+Jumbo+LoRA, $J=6$, rank=8	8.1K	88.8	3.95	44.94
ViT+Jumbo+LoRA, $J=6$, rank=32	8.1K	90.1	3.64	44.97

Results. Our method is robust to the choice of Jumbo multiplier and inner Jumbo FFN multiplier (Tab. 2), although generally, higher multipliers perform better on ImageNet-1K. For simplicity, we use the largest multipliers as the defaults (gray) and use them in our apples-to-apples comparisons (i.e., subsections 4.1 and 4.2). However, lower values may provide slightly better accuracy-speed trade-offs. Please see Appendix A.2.3 for complete results.

5. Discussion

Limitations. Jumbo’s most significant limitation is the parameter increase due to dedicating a separate FFN to the Jumbo CLS token (instead of sharing parameters between patches) and increasing the size of this Jumbo FFN. For many applications, increasing speed is more helpful than increasing memory is harmful. For memory-constrained applications, we propose a solution to control this cost: tie Jumbo’s FFN parameters across layers. This strategy results in a $12\times$ reduction in additional model parameters (our models have 12 layers). We also experiment with applying layer-specific LoRAs (Hu et al., 2022) to the tied Jumbo parameters; this is a parameter-efficient means of enabling the Jumbo FFNs to differ across layers and is similar to Li et al. (2024a). We find that both methods are highly effective at controlling Jumbo’s parameter count (Tab. 3).

Conclusion. Jumbo is a highly promising and elegantly simple method that increases the global reasoning capacity of plain ViTs while maintaining throughput. Jumbo is most helpful when the patch token width is otherwise too narrow for the task; we demonstrate this by decreasing the patch token width and, separately, increasing the output dimensionality. There are many exciting ways to apply Jumbo, such as zero-shot image classification, which can have large output vocabularies that we expect Jumbo to better model. There are also many ways to extend Jumbo, for example, by including multiple shared Jumbo tokens (e.g., two shared $J=2$ Jumbo tokens) or parameter-efficient alternatives to dense linear layers to control memory costs further (Qiu et al., 2024).

Impact Statement

This work presents new designs and empirical results for deep network architectures for more accurate and computationally efficient modeling applied to visual recognition and time series processing. This general topic does not have more specific societal consequences aside from those inherited, good or bad, from the adoption of machine learning.

References

- Akbari, H., Yuan, L., Qian, R., Chuang, W.-H., Chang, S.-F., Cui, Y., and Gong, B. Vatt: Transformers for multimodal self-supervised learning from raw video, audio and text. *Advances in Neural Information Processing Systems*, 34: 24206–24221, 2021.
- Alabdulmohsin, I. M., Zhai, X., Kolesnikov, A., and Beyer, L. Getting vit in shape: Scaling laws for compute-optimal model design. *Advances in Neural Information Processing Systems*, 36, 2024.
- Assran, M., Duval, Q., Misra, I., Bojanowski, P., Vincent, P., Rabbat, M., LeCun, Y., and Ballas, N. Self-supervised learning from images with a joint-embedding predictive architecture. In *Proceedings of the IEEE/CVF Conference on Computer Vision and Pattern Recognition*, pp. 15619–15629, 2023.
- Bagnall, A., Dau, H. A., Lines, J., Flynn, M., Large, J., Bostrom, A., Southam, P., and Keogh, E. The uea multivariate time series classification archive, 2018. URL <https://arxiv.org/abs/1811.00075>.
- Bai, J., Bai, S., Yang, S., Wang, S., Tan, S., Wang, P., Lin, J., Zhou, C., and Zhou, J. Qwen-vl: A versatile vision-language model for understanding, localization, text reading, and beyond. *arXiv preprint arXiv:2308.12966*, 2023.
- Beyer, L., Hénaff, O. J., Kolesnikov, A., Zhai, X., and Oord, A. v. d. Are we done with imagenet? *arXiv preprint arXiv:2006.07159*, 2020.
- Beyer, L., Zhai, X., Royer, A., Markeeva, L., Anil, R., and Kolesnikov, A. Knowledge distillation: A good teacher is patient and consistent. In *Proceedings of the IEEE/CVF conference on computer vision and pattern recognition*, pp. 10925–10934, 2022.
- Beyer, L., Izmailov, P., Kolesnikov, A., Caron, M., Kornblith, S., Zhai, X., Minderer, M., Tschannen, M., Alabdulmohsin, I., and Pavetic, F. Flexivit: One model for all patch sizes. In *Proceedings of the IEEE/CVF Conference on Computer Vision and Pattern Recognition*, pp. 14496–14506, 2023.
- Cai, H., Li, J., Hu, M., Gan, C., and Han, S. Efficientvit: Lightweight multi-scale attention for high-resolution dense prediction. In *Proceedings of the IEEE/CVF International Conference on Computer Vision*, pp. 17302–17313, 2023.
- Chen, Y., Dai, X., Chen, D., Liu, M., Dong, X., Yuan, L., and Liu, Z. Mobile-former: Bridging mobilenet and transformer. In *Proceedings of the IEEE/CVF conference on computer vision and pattern recognition*, pp. 5270–5279, 2022.
- Choy, C., Gwak, J., and Savarese, S. 4d spatio-temporal convnets: Minkowski convolutional neural networks. In *Proceedings of the IEEE/CVF conference on computer vision and pattern recognition*, pp. 3075–3084, 2019.
- Cubuk, E. D., Zoph, B., Mane, D., Vasudevan, V., and Le, Q. V. Autoaugment: Learning augmentation policies from data. *arXiv preprint arXiv:1805.09501*, 2018.
- Dao, T. Flashattention-2: Faster attention with better parallelism and work partitioning. *arXiv preprint arXiv:2307.08691*, 2023.
- Dao, T., Fu, D., Ermon, S., Rudra, A., and Ré, C. Flashattention: Fast and memory-efficient exact attention with io-awareness. *Advances in Neural Information Processing Systems*, 35:16344–16359, 2022.
- Darcet, T., Oquab, M., Mairal, J., and Bojanowski, P. Vision transformers need registers. In *The Twelfth International Conference on Learning Representations*, 2024. URL <https://openreview.net/forum?id=2dnO3LLiJ1>.
- Dau, H. A., Bagnall, A. J., Kamgar, K., Yeh, C. M., Zhu, Y., Gharghabi, S., Ratanamahatana, C. A., and Keogh, E. J. The UCR time series archive. *arXiv preprint arXiv:1810.07758*, 2018.
- Dehghani, M., Djolonga, J., Mustafa, B., Padlewski, P., Heek, J., Gilmer, J., Steiner, A. P., Caron, M., Geirhos, R., Alabdulmohsin, I., et al. Scaling vision transformers to 22 billion parameters. In *International Conference on Machine Learning*, pp. 7480–7512. PMLR, 2023.
- Dehghani, M., Mustafa, B., Djolonga, J., Heek, J., Minderer, M., Caron, M., Steiner, A., Puigcerver, J., Geirhos, R., Alabdulmohsin, I. M., et al. Patch n’pack: Navit, a vision transformer for any aspect ratio and resolution. *Advances in Neural Information Processing Systems*, 36, 2024.
- Deng, J., Dong, W., Socher, R., Li, L.-J., Li, K., and Fei-Fei, L. Imagenet: A large-scale hierarchical image database. In *2009 IEEE conference on computer vision and pattern recognition*, pp. 248–255. Ieee, 2009.
- Dong, X., Fu, Y., Diao, S., Byeon, W., Chen, Z., Mahabaleshwar, A. S., Liu, S.-Y., Keirsbilck, M. V., Chen,

- M.-H., Suhara, Y., Lin, Y., Kautz, J., and Molchanov, P. Hymba: A hybrid-head architecture for small language models, 2024. URL <https://arxiv.org/abs/2411.13676>.
- Dosovitskiy, A., Beyer, L., Kolesnikov, A., Weissenborn, D., Zhai, X., Unterthiner, T., Dehghani, M., Minderer, M., Heigold, G., Gelly, S., Uszkoreit, J., and Houlsby, N. An image is worth 16x16 words: Transformers for image recognition at scale. In *International Conference on Learning Representations*, 2021. URL <https://openreview.net/forum?id=YicbFdNTTy>.
- Dou, Z.-Y., Xu, Y., Gan, Z., Wang, J., Wang, S., Wang, L., Zhu, C., Zhang, P., Yuan, L., Peng, N., et al. An empirical study of training end-to-end vision-and-language transformers. In *Proceedings of the IEEE/CVF Conference on Computer Vision and Pattern Recognition*, pp. 18166–18176, 2022.
- Elhage, N., Nanda, N., Olsson, C., Henighan, T., Joseph, N., Mann, B., Askell, A., Bai, Y., Chen, A., Conerly, T., DasSarma, N., Drain, D., Ganguli, D., Hatfield-Dodds, Z., Hernandez, D., Jones, A., Kernion, J., Lovitt, L., Ndousse, K., Amodei, D., Brown, T., Clark, J., Kaplan, J., McCandlish, S., and Olah, C. A mathematical framework for transformer circuits. *Transformer Circuits Thread*, 2021. <https://transformer-circuits.pub/2021/framework/index.html>.
- Fan, H., Xiong, B., Mangalam, K., Li, Y., Yan, Z., Malik, J., and Feichtenhofer, C. Multiscale vision transformers. In *Proceedings of the IEEE/CVF international conference on computer vision*, pp. 6824–6835, 2021.
- Fang, Y., Yang, S., Wang, S., Ge, Y., Shan, Y., and Wang, X. Unleashing vanilla vision transformer with masked image modeling for object detection. In *Proceedings of the IEEE/CVF International Conference on Computer Vision*, pp. 6244–6253, 2023.
- Fu, L., Lian, L., Wang, R., Shi, B., Wang, X., Yala, A., Darrell, T., Efros, A. A., and Goldberg, K. Rethinking patch dependence for masked autoencoders. *arXiv preprint arXiv:2401.14391*, 2024.
- Fuller, A., Kyrollos, D., Yassin, Y., and Green, J. R. Lookhere: Vision transformers with directed attention generalize and extrapolate. In *The Thirty-eighth Annual Conference on Neural Information Processing Systems*, 2024. URL <https://openreview.net/forum?id=o7DOGbZeyP>.
- Garrido, Q., Assran, M., Ballas, N., Bardes, A., Najman, L., and LeCun, Y. Learning and leveraging world models in visual representation learning. *arXiv preprint arXiv:2403.00504*, 2024.
- Grover, S., Jalali, A., and Etemad, A. Segment, shuffle, and stitch: A simple layer for improving time-series representations. In *The Thirty-eighth Annual Conference on Neural Information Processing Systems*, 2024. URL <https://openreview.net/forum?id=zmlLcgRpHm>.
- Han, K., Wang, Y., Tian, Q., Guo, J., Xu, C., and Xu, C. Ghostnet: More features from cheap operations. In *Proceedings of the IEEE/CVF conference on computer vision and pattern recognition*, pp. 1580–1589, 2020.
- He, K., Zhang, X., Ren, S., and Sun, J. Deep residual learning for image recognition. In *Proceedings of the IEEE conference on computer vision and pattern recognition*, pp. 770–778, 2016.
- He, K., Chen, X., Xie, S., Li, Y., Dollár, P., and Girshick, R. Masked autoencoders are scalable vision learners. In *Proceedings of the IEEE/CVF conference on computer vision and pattern recognition*, pp. 16000–16009, 2022.
- Hendrycks, D. and Gimpel, K. Bridging nonlinearities and stochastic regularizers with gaussian error linear units. *arXiv preprint arXiv:1606.08415*, 2016.
- Hendrycks, D., Basart, S., Mu, N., Kadavath, S., Wang, F., Dorundo, E., Desai, R., Zhu, T., Parajuli, S., Guo, M., et al. The many faces of robustness: A critical analysis of out-of-distribution generalization. In *Proceedings of the IEEE/CVF international conference on computer vision*, pp. 8340–8349, 2021.
- Heo, B., Park, S., Han, D., and Yun, S. Rotary position embedding for vision transformer. In *European Conference on Computer Vision*, pp. 289–305. Springer, 2025.
- Howard, A., Sandler, M., Chu, G., Chen, L.-C., Chen, B., Tan, M., Wang, W., Zhu, Y., Pang, R., Vasudevan, V., et al. Searching for mobilenetv3. In *Proceedings of the IEEE/CVF international conference on computer vision*, pp. 1314–1324, 2019.
- Howard, A. G. Mobilenets: Efficient convolutional neural networks for mobile vision applications. *arXiv preprint arXiv:1704.04861*, 2017.
- Hu, E. J., yelong shen, Wallis, P., Allen-Zhu, Z., Li, Y., Wang, S., Wang, L., and Chen, W. LoRA: Low-rank adaptation of large language models. In *International Conference on Learning Representations*, 2022. URL <https://openreview.net/forum?id=nZeVKeeFYf9>.
- Hu, Y., Wang, X., Wu, L., Zhang, H., Li, S. Z., Wang, S., and Chen, T. Fm-ts: Flow matching for time series generation. *arXiv preprint arXiv:2411.07506*, 2024.

- Le, X.-M., Luo, L., Aickelin, U., and Tran, M.-T. Shapeformer: Shapelet transformer for multivariate time series classification. In *Proceedings of the 30th ACM SIGKDD Conference on Knowledge Discovery and Data Mining*, KDD '24, pp. 1484–1494, New York, NY, USA, 2024. Association for Computing Machinery. doi: 10.1145/3637528.3671862. URL <https://doi.org/10.1145/3637528.3671862>.
- Leigh, M., Klein, S., Charton, F., Golling, T., Heinrich, L., Kagan, M., Ochoa, I., and Osadchy, M. Is tokenization needed for masked particle modelling? *arXiv preprint arXiv:2409.12589*, 2024.
- Li, J., Nie, Q., Fu, W., Lin, Y., Tao, G., Liu, Y., and Wang, C. Lora: Low-rank residual structure for parameter-efficient network stacking. In *Proceedings of the IEEE/CVF Conference on Computer Vision and Pattern Recognition*, pp. 15866–15876, 2024a.
- Li, X., Ding, H., Yuan, H., Zhang, W., Pang, J., Cheng, G., Chen, K., Liu, Z., and Loy, C. C. Transformer-based visual segmentation: A survey. *IEEE Transactions on Pattern Analysis and Machine Intelligence*, 2024b.
- Li, Y., Mao, H., Girshick, R., and He, K. Exploring plain vision transformer backbones for object detection. In *European conference on computer vision*, pp. 280–296. Springer, 2022a.
- Li, Y., Yuan, G., Wen, Y., Hu, J., Evangelidis, G., Tulyakov, S., Wang, Y., and Ren, J. Efficientformer: Vision transformers at mobilenet speed. *Advances in Neural Information Processing Systems*, 35:12934–12949, 2022b.
- Li, Y., Hu, J., Wen, Y., Evangelidis, G., Salahi, K., Wang, Y., Tulyakov, S., and Ren, J. Rethinking vision transformers for mobilenet size and speed. In *Proceedings of the IEEE/CVF International Conference on Computer Vision*, pp. 16889–16900, 2023.
- Liu, H., Li, C., Wu, Q., and Lee, Y. J. Visual instruction tuning, 2023a.
- Liu, S., Zeng, Z., Ren, T., Li, F., Zhang, H., Yang, J., Jiang, Q., Li, C., Yang, J., Su, H., et al. Grounding dino: Marrying dino with grounded pre-training for open-set object detection. In *European Conference on Computer Vision*, pp. 38–55. Springer, 2025.
- Liu, W., Zhu, F., Ma, S., and Liu, C.-L. MSPE: Multi-scale patch embedding prompts vision transformers to any resolution. In *The Thirty-eighth Annual Conference on Neural Information Processing Systems*, 2024. URL <https://openreview.net/forum?id=9Q9UiAyV40>.
- Liu, Y., Matsoukas, C., Strand, F., Azizpour, H., and Smith, K. Patchdropout: Economizing vision transformers using patch dropout. In *Proceedings of the IEEE/CVF Winter Conference on Applications of Computer Vision*, pp. 3953–3962, 2023b.
- Liu, Z., Lin, Y., Cao, Y., Hu, H., Wei, Y., Zhang, Z., Lin, S., and Guo, B. Swin transformer: Hierarchical vision transformer using shifted windows. In *Proceedings of the IEEE/CVF international conference on computer vision*, pp. 10012–10022, 2021.
- Liu, Z., Mao, H., Wu, C.-Y., Feichtenhofer, C., Darrell, T., and Xie, S. A convnet for the 2020s. In *Proceedings of the IEEE/CVF conference on computer vision and pattern recognition*, pp. 11976–11986, 2022.
- Loshchilov, I. Decoupled weight decay regularization. *arXiv preprint arXiv:1711.05101*, 2017.
- Mehta, S. and Rastegari, M. Mobilevit: light-weight, general-purpose, and mobile-friendly vision transformer. *arXiv preprint arXiv:2110.02178*, 2021.
- Mehta, S. and Rastegari, M. Separable self-attention for mobile vision transformers. *arXiv preprint arXiv:2206.02680*, 2022.
- Messaoud, K., Cord, M., and Alahi, A. Towards generalizable trajectory prediction using dual-level representation learning and adaptive prompting. *arXiv preprint arXiv:2501.04815*, 2025.
- Muhammad, K., Ullah, A., Lloret, J., Del Ser, J., and de Albuquerque, V. H. C. Deep learning for safe autonomous driving: Current challenges and future directions. *IEEE Transactions on Intelligent Transportation Systems*, 22(7):4316–4336, 2020.
- Nie, Y., H. Nguyen, N., Sinthong, P., and Kalagnanam, J. A time series is worth 64 words: Long-term forecasting with transformers. In *International Conference on Learning Representations*, 2023.
- Omranpour, S., Rabusseau, G., and Rabbany, R. Higher order transformers: Enhancing stock movement prediction on multimodal time-series data. *arXiv preprint arXiv:2412.10540*, 2024.
- Pan, J., Bulat, A., Tan, F., Zhu, X., Dudziak, L., Li, H., Tzimiropoulos, G., and Martinez, B. Edgevits: Competing light-weight cnns on mobile devices with vision transformers. In *European Conference on Computer Vision*, pp. 294–311. Springer, 2022.
- Paszke, A., Gross, S., Massa, F., Lerer, A., Bradbury, J., Chanan, G., Killeen, T., Lin, Z., Gimelshein, N., Antiga, L., et al. Pytorch: An imperative style, high-performance

- deep learning library. *Advances in neural information processing systems*, 32, 2019.
- Qin, D., Leichner, C., Delakis, M., Fornoni, M., Luo, S., Yang, F., Wang, W., Banbury, C., Ye, C., Akin, B., et al. Mobilenetv4: Universal models for the mobile ecosystem. In *European Conference on Computer Vision*, pp. 78–96. Springer, 2025.
- Qiu, S., Potapczynski, A., Finzi, M., Goldblum, M., and Wilson, A. G. Compute Better Spent: Replacing Dense Layers with Structured Matrices. *International Conference on Machine Learning (ICML)*, 2024.
- Radford, A., Kim, J. W., Hallacy, C., Ramesh, A., Goh, G., Agarwal, S., Sastry, G., Askell, A., Mishkin, P., Clark, J., et al. Learning transferable visual models from natural language supervision. In *International conference on machine learning*, pp. 8748–8763. PMLR, 2021.
- Recht, B., Roelofs, R., Schmidt, L., and Shankar, V. Do imagenet classifiers generalize to imagenet? In *International conference on machine learning*, pp. 5389–5400. PMLR, 2019.
- Ridnik, T., Ben-Baruch, E., Noy, A., and Zelnik-Manor, L. Imagenet-21k pretraining for the masses. In *Thirty-fifth Conference on Neural Information Processing Systems Datasets and Benchmarks Track (Round 1)*, 2021. URL https://openreview.net/forum?id=Zkj_VcZ6ol.
- Rolf, E., Klemmer, K., Robinson, C., and Kerner, H. Position: Mission critical – satellite data is a distinct modality in machine learning. In *Proceedings of the 41st International Conference on Machine Learning*, pp. 42691–42706, 2024.
- Russakovsky, O., Deng, J., Su, H., Krause, J., Satheesh, S., Ma, S., Huang, Z., Karpathy, A., Khosla, A., Bernstein, M., et al. Imagenet large scale visual recognition challenge. *International journal of computer vision*, 115: 211–252, 2015.
- Ryali, C., Hu, Y.-T., Bolya, D., Wei, C., Fan, H., Huang, P.-Y., Aggarwal, V., Chowdhury, A., Poursaeed, O., Hoffman, J., et al. Hiera: A hierarchical vision transformer without the bells-and-whistles. In *International Conference on Machine Learning*, pp. 29441–29454. PMLR, 2023.
- Sandler, M., Howard, A., Zhu, M., Zhmoginov, A., and Chen, L.-C. Mobilenetv2: Inverted residuals and linear bottlenecks. In *Proceedings of the IEEE conference on computer vision and pattern recognition*, pp. 4510–4520, 2018.
- Shah, J., Bikshandi, G., Zhang, Y., Thakkar, V., Ramani, P., and Dao, T. Flashattention-3: Fast and accurate attention with asynchrony and low-precision. *arXiv preprint arXiv:2407.08608*, 2024.
- Simonyan, K. Very deep convolutional networks for large-scale image recognition. *arXiv preprint arXiv:1409.1556*, 2014.
- Steiner, A. P., Kolesnikov, A., Zhai, X., Wightman, R., Uszkoreit, J., and Beyer, L. How to train your vit? data, augmentation, and regularization in vision transformers. *Transactions on Machine Learning Research*, 2022. ISSN 2835-8856. URL <https://openreview.net/forum?id=4nPswr1KcP>.
- Tan, M., Chen, B., Pang, R., Vasudevan, V., Sandler, M., Howard, A., and Le, Q. V. Mnasnet: Platform-aware neural architecture search for mobile. In *Proceedings of the IEEE/CVF conference on computer vision and pattern recognition*, pp. 2820–2828, 2019.
- Thimonier, H., Costa, J. L. D. M., Popineau, F., Rimmel, A., and Doan, B.-L. T-jepa: Augmentation-free self-supervised learning for tabular data. *arXiv preprint arXiv:2410.05016*, 2024.
- Touvron, H., Vedaldi, A., Douze, M., and Jégou, H. Fixing the train-test resolution discrepancy. *Advances in neural information processing systems*, 32, 2019.
- Touvron, H., Cord, M., and Jégou, H. Deit iii: Revenge of the vit. In *European conference on computer vision*, pp. 516–533. Springer, 2022.
- Vaquero, L., Xu, Y., Alameda-Pineda, X., Brea, V. M., and Mucientes, M. Lost and found: Overcoming detector failures in online multi-object tracking. In *European Conference on Computer Vision*, pp. 448–466. Springer, 2024.
- Vasu, P. K. A., Gabriel, J., Zhu, J., Tuzel, O., and Ranjan, A. Mobileone: An improved one millisecond mobile backbone. In *Proceedings of the IEEE/CVF conference on computer vision and pattern recognition*, pp. 7907–7917, 2023a.
- Vasu, P. K. A., Gabriel, J., Zhu, J., Tuzel, O., and Ranjan, A. Fastvit: A fast hybrid vision transformer using structural reparameterization. In *Proceedings of the IEEE/CVF International Conference on Computer Vision*, 2023b.
- Wei, Y., Gupta, A., and Morgado, P. Towards latent masked image modeling for self-supervised visual representation learning. In *European Conference on Computer Vision*, pp. 1–17. Springer, 2025.

- Weinzaepfel, P., Lucas, T., Leroy, V., Cabon, Y., Arora, V., Brégier, R., Csurka, G., Antsfeld, L., Chidlovskii, B., and Revaud, J. Croco v2: Improved cross-view completion pre-training for stereo matching and optical flow. In *Proceedings of the IEEE/CVF International Conference on Computer Vision*, pp. 17969–17980, 2023.
- Wightman, R. Pytorch image models. <https://github.com/rwightman/pytorch-image-models>, 2019.
- Woo, S., Debnath, S., Hu, R., Chen, X., Liu, Z., Kweon, I. S., and Xie, S. Convnext v2: Co-designing and scaling convnets with masked autoencoders. In *Proceedings of the IEEE/CVF Conference on Computer Vision and Pattern Recognition*, pp. 16133–16142, 2023.
- Xu, P., Zhu, X., and Clifton, D. A. Multimodal learning with transformers: A survey. *IEEE Transactions on Pattern Analysis and Machine Intelligence*, 45(10):12113–12132, 2023.
- Yun, S. and Ro, Y. Shvit: Single-head vision transformer with memory efficient macro design. In *Proceedings of the IEEE/CVF Conference on Computer Vision and Pattern Recognition (CVPR)*, pp. 5756–5767, 2024.
- Zerveas, G., Jayaraman, S., Patel, D., Bhamidipaty, A., and Eickhoff, C. A transformer-based framework for multivariate time series representation learning. In *Proceedings of the 27th ACM SIGKDD Conference on Knowledge Discovery & Data Mining, KDD '21*, pp. 2114–2124, 2021.
- Zhai, X., Kolesnikov, A., Houlsby, N., and Beyer, L. Scaling vision transformers. In *Proceedings of the IEEE/CVF conference on computer vision and pattern recognition*, pp. 12104–12113, 2022.
- Zhang, B., Tian, Z., Tang, Q., Chu, X., Wei, X., Shen, C., et al. Segvit: Semantic segmentation with plain vision transformers. *Advances in Neural Information Processing Systems*, 35:4971–4982, 2022.

A. Appendix

A.1. Compute-efficient Architecture Descriptions

① EfficientViT (Cai et al., 2023) is a hierarchical architecture with four stages and one head. Stages 1 and 2 consist of MBConv layers (Sandler et al., 2018). Stages 3 and 4 consist of MBConv sublayers and their novel EfficientViT sublayer, consisting of an efficient attention module and an FFN+DWConv module (Howard, 2017). Their attention module creates queries, keys, and values of three scales via three DWConvs, and then each set of queries, keys, and values undergoes efficient linear attention. Finally, the head receives outputs from Stages 2, 3, and 4, and applies a final MBConv. EfficientViT variants differ in stage depths and widths, as well as head width.

② SHViT (Yun & Ro, 2024) is a hierarchical architecture with three stages. Stage 1 consists of a DWConv+BatchNorm sublayer and an FFN sublayer. Stages 2 and 3 incorporate their novel single-headed self-attention (SHSA) sublayer between the stage 1 sublayers. SHSA consists of performing single-headed self-attention on a fraction of dimensions (1/4.67 ratio); the other dimensions pass straight through, further reducing cost. Both FFN and SHSA sublayers also replace linear layers with DWConv. SHViT variants differ in stage depths and widths.

③ MobileNetV4 (Qin et al., 2025) variants use their FusedIB, ExtraDW, and Mobile MQA (multi-query attention) modules along with MBConv, ConvNext-Like (Liu et al., 2022), and FFN modules. Variants differ in stage depths and widths, the number of stages, and stage architectures built with a combination of the listed modules.

A.2. Experimental Details

A.2.1. IMAGENET-1K AND -21K HYPERPARAMETERS

We pick these recipes based on findings in the literature — such as Touvron et al. (2022), Fuller et al. (2024), Beyer et al. (2022), Dehghani et al. (2024), and Steiner et al. (2022) — and past experience indicating that these recipes would result in strong models.

ImageNet-1K training recipe: 128×128 px images, 400 epochs, 1024 batch size, PyTorch’s AdamW optimizer with a 0.05 weight decay, 1.0 clip grad norm, `deit3-base-patch16-224.fb-in22k-ft-in1k` teacher (Touvron et al., 2022) given 224×224 px images using Wightman (2019)’s implementation, KL divergence loss between student and teacher logits (Beyer et al., 2022), linear learning rate warmup for 10% of steps to $\{1e-3, 3e-3\}$ and cooldown using a cosine decay schedule to $1e-5$, mixup $\alpha = 0.8$, cutmix $\alpha = 1$, and 3-Augment data augmentation (Touvron et al., 2022).

ImageNet-1K finetuning recipe: 224×224 px images, 20 epochs, 512 batch size, PyTorch’s AdamW optimizer with a 0.1 weight decay, 1.0 clip grad norm, `deit3-large-patch16-224.fb-in22k-ft-in1k` teacher (Touvron et al., 2022) given 224×224 px images using Wightman (2019)’s implementation, KL divergence loss between student and teacher logits (Beyer et al., 2022), linear learning rate warmup for 25% of steps to $5e-5$ and cooldown using a cosine decay schedule to $1e-5$, mixup $\alpha = 0.8$, cutmix $\alpha = 1$, and AutoAugment (“`rand-m9-mstd0.5-inc1`”) data augmentation (Cubuk et al., 2018) following DEIT III’s (Touvron et al., 2022) high-res finetuning recipe.

ImageNet-21K training recipe: 224×224 px images, 50 epochs, 1024 batch size, PyTorch’s AdamW optimizer with a 0.02 weight decay, 1.0 clip grad norm, cross-entropy loss, linear learning rate warmup for 10% of steps to $3e-3$ and cooldown using a cosine decay schedule to $1e-5$, mixup $\alpha = 0.8$, cutmix $\alpha = 0$, and 3-Augment data augmentation (Touvron et al., 2022). To speed up training, we also employ a token dropping strategy starting at 90%, linearly decreasing to 10%.

A.2.2. TIME SERIES EXPERIMENTS

We adopt the PatchTST (Nie et al., 2023) architecture for our time series experiments. PatchTST is a patch-based transformer architecture for time series processing. The method splits a univariate time series into patches processed as they are in ViTs for classification, aside from position encoding (2D vs. 1D). For multivariate series, each channel is processed *independently* using the shared transformer backbone, with the final-layer CLS tokens from each channel concatenated before classification. We extend this shared backbone with registers (PatchTST+Registers) and Jumbo (PatchTST+Jumbo).

We closely follow the PatchTST training recipe for our experiments, making minor adjustments based on prior experience to enhance performance. This method remains competitive with recent transformer-based benchmarks for time series classification (Zerveas et al., 2021; Grover et al., 2024; Le et al., 2024). Apart from variations in time series length, all

experiments use the same hyperparameters and methodology.

PatchTST Hyperparameters: The model comprises 3 encoder layers, each with 16 attention heads and a token width of $D = 128$. The transformer FFN includes two linear layers with a GELU activation (Hendrycks & Gimpel, 2016); the first expands the hidden dimension to 256, while the second projects it back to 128. For PatchTST+Jumbo, we use $J = 4$. For PatchTST+Registers, R is calculated according to Appendix A.2.3.

Time Series training recipe: We perform a hyperparameter sweep over the Cartesian product of learning rates $\{3e-3, 1e-3, 3e-4, 1e-4\}$ and dropout rates $\{0.0, 0.1, 0.2\}$. Each configuration uses either 8 or 42 equally sized patches of maximum possible length, with end-padding applied as needed. The stride length is set to half the patch length. Unless stated otherwise, all experiments follow the same setup: 100 epochs, 256 batch size, PyTorch’s AdamW optimizer with a 0.02 weight decay, cross-entropy loss, and a linear learning rate warmup for the first 10% of steps, followed by a cooldown using cosine decay to $1e-8$. For large datasets, we reduce the number of epochs to ensure efficient processing within a reasonable time frame; specifically, we train datasets {Sleep, Tiselas, FaceDetection} for 20 epochs.

Each dataset from the UEA and UCR archives includes a prescribed validation set. We create a new 50/50 test/validation split from each of these original validation sets, selecting the best run based on validation performance. All reported results are from the *test* set.

The 20 datasets were selected in decreasing order of their number of training examples; datasets with either (i) fewer than 42 total timesteps or (ii) significant data preparation issues were excluded.

A.2.3. FLOP DETAILS

To ensure a fair comparison, we configure PatchTST+Registers and PatchTST+Jumbo to have approximately equal per-layer FLOPs by selecting the number of registers R in the former and the Jumbo multiplier J in the latter accordingly. Additionally, we apply average pooling to the J split segments of the Jumbo token to prevent a significant increase in the number of learnable parameters of the classification head. This pooling produces a token of width D per channel before concatenation, effectively serving the same role as a CLS token. The detailed per-layer FLOP calculation is provided by the proposition below.

Proposition 1. Let P be the total number of local patch tokens, R the number of register tokens, D the width, and J the Jumbo multiplier. Given an FFN hidden dimension of $2D$, and otherwise fixed parameters, a Register architecture with R registers has the same per-layer FLOP count as a Jumbo architecture with multiplier J if and only if

$$R = -(2D + P) + \sqrt{(2D + P)^2 + (1 + 2D)J^2 + 2(D + P)J}$$

Proof. Let F denote the FLOP count. Given a sequence length of n tokens, each of width d , the FLOP contributions from the MHSA and FFN sublayers in a single transformer layer with a FFN hidden dimension of ld are given by

$$F_{\text{MHSA}} = 4nd^2 + 2n^2d \text{ and } F_{\text{FFN}} = l^2nd^2 = 4nd^2$$

where we fix $l = 2$. For the Register architecture, $n = P + R$ and $d = D$ for both the MHSA and the FFN contributions. For the Jumbo architecture, $n = P + J$ and $d = D$ for MHSA. The FFN contribution is split; local patch tokens contribute with $n = P, d = D$ while the dedicated Jumbo FFN has $n = 1, d = JD$. From summing the contributions, it follows that

$$\begin{aligned} F_{\text{Reg}} &= 4(P + R)D^2 + 2(P + R)^2D + 4(P + R)D^2 \\ F_{\text{Jumbo}} &= 4(P + R)D^2 + 2(P + R)D^2 + 4PD^2 + 4J^2D^2 \end{aligned}$$

Equating $F_{\text{Reg}} = F_{\text{Jumbo}}$ and solving for R gives the stated result. □

In our time series experiments, we compute R , rounding to the nearest integer, to match the per-layer FLOP count of a Jumbo architecture with multiplier J as closely as possible.

Table 4. ViT+Jumbo ablation results, obtained on 128×128 px images (%).

Patch Width	Jumbo Multiplier	Inner FFN Multiplier	Throughput 128^2 px	Throughput 224^2 px	ImageNet-Val		ImageNet-Real		ImageNet-v2		ImageNet-HR		ImageNet-R		
					Top-1	Top-5	Top-1	Top-5	Top-1	Top-5	Top-1	Top-5	Top-1	Top-5	
192	2	2	71.6K	21.6K	70.0	89.6	77.5	93.1	57.3	80.0	26.1	40.9	79.3	93.2	
		4	69.6K	21.5K	70.4	89.6	77.8	93.1	57.3	79.8	25.5	39.6	79.7	93.3	
	4	1	69.6K	21.3K	71.5	90.4	78.8	93.7	59.2	81.3	26.9	41.7	80.8	93.7	
		2	68.1K	21.2K	70.6	89.6	77.6	93.0	57.7	79.8	25.9	40.3	80.4	93.5	
	6	4	64.9K	20.8K	72.2	90.6	79.2	93.6	59.3	81.1	26.6	41.2	81.8	94.1	
		1	65.3K	20.9K	72.1	90.5	79.2	93.7	58.9	81.1	26.4	41.1	80.8	94.2	
		2	63.5K	20.6K	71.8	90.2	78.7	93.3	58.2	80.6	25.8	39.8	80.7	93.6	
		4	56.5K	19.9K	73.0	90.7	79.6	93.7	59.4	81.2	26.8	41.3	82.3	93.9	
	384	2	2	27.2K	8.7K	77.0	93.5	83.6	96.0	64.6	85.8	31.9	47.9	85.8	96.4
			4	26.1K	8.6K	78.1	94.0	84.4	96.3	65.9	86.1	32.8	48.7	86.1	96.4
4		1	26.1K	8.6K	77.3	93.6	83.7	96.0	64.9	85.8	32.1	47.8	86.5	96.2	
		2	24.5K	8.5K	77.9	93.9	84.0	96.3	65.7	85.9	32.7	48.6	86.7	96.2	
6		4	23.6K	8.3K	77.9	93.8	84.0	96.2	65.7	85.8	32.4	48.0	86.2	96.2	
		1	23.9K	8.4K	77.6	93.6	84.0	96.1	65.8	85.8	32.1	47.9	86.7	96.2	
		2	22.9K	8.2K	77.8	93.6	83.8	96.0	65.0	85.3	32.2	47.5	86.6	96.0	
		4	19.5K	7.8K	78.3	93.8	84.2	96.1	66.1	86.0	32.9	48.6	87.0	96.3	

Table 5. ViT+Registers results, obtained on 128×128 px images (%).

Patch Width	Num. Registers	Learning Rate	Throughput imgs/s	ImageNet-Val		ImageNet-ReaL		ImageNet-v2		ImageNet-R		ImageNet-HR	
				Top-1	Top-5	Top-1	Top-5	Top-1	Top-5	Top-1	Top-5	Top-1	Top-5
128	16	$3e-3$	105.9K	53.6	78.5	60.8	83.6	42.4	67.8	15.9	28.6	61.9	83.4
	16	$1e-3$		51.9	76.8	59.0	81.8	40.8	65.4	13.7	24.9	60.5	82.6
192	8	$3e-3$	59.9K	68.5	88.8	76.1	92.6	55.7	78.8	24.9	39.4	77.8	92.2
	16	$3e-3$	52.2K	68.8	88.9	76.6	92.6	55.9	79.4	24.8	38.9	78.5	92.5
	16	$1e-3$		66.1	87.2	74.0	91.2	54.2	77.0	22.9	36.2	75.4	91.6
384	8	$3e-3$	24.4K	77.8	93.9	84.3	96.2	65.8	86.3	33.3	48.6	86.8	96.5
	16	$3e-3$	22.2K	78.1	94.0	84.5	96.3	66.1	86.6	33.3	48.6	86.6	96.5
	16	$1e-3$		78.2	94.1	84.5	96.3	66.4	86.6	33.5	48.4	87.2	96.6

Table 6. ViT+Jumbo results, obtained on 128×128 px images (%).

Patch Width	Learning Rate	Throughput imgs/s	ImageNet-Val		ImageNet-ReaL		ImageNet-v2		ImageNet-R		ImageNet-HR	
			Top-1	Top-5	Top-1	Top-5	Top-1	Top-5	Top-1	Top-5	Top-1	Top-5
96	$3e-3$	133.3K	64.0	84.9	71.2	88.8	50.6	74.0	19.8	32.7	72.7	89.5
	$1e-3$		63.2	84.5	70.3	88.5	49.8	72.9	18.7	31.1	72.0	88.8
128	$3e-3$	101.7K	68.2	87.7	75.2	91.3	55.0	77.4	23.2	36.7	77.3	92.1
	$1e-3$		68.8	88.1	75.6	91.5	55.1	77.5	22.8	36.5	77.9	92.0
192	$3e-3$	56.5K	73.0	90.7	79.6	93.7	59.4	81.2	26.8	41.3	82.3	93.9
	$1e-3$		72.6	90.6	79.2	93.5	58.8	80.5	25.7	39.8	81.6	94.1
384	$3e-3$	19.5K	78.3	93.8	84.2	96.1	66.1	86.0	32.9	48.6	87.0	96.3
	$1e-3$		78.5	94.2	84.4	96.3	65.8	86.4	33.0	48.7	87.2	96.3

Table 7. MobileNetV4 results, obtained on 128×128 px images (%).

Size	Learning Rate	Throughput imgs/s	ImageNet-Val		ImageNet-ReaL		ImageNet-v2		ImageNet-R		ImageNet-HR	
			Top-1	Top-5	Top-1	Top-5	Top-1	Top-5	Top-1	Top-5	Top-1	Top-5
conv-small	$3e-3$	135.7K	62.1	83.6	69.2	88.1	49.1	72.8	20.4	34.3	71.8	89.4
	$1e-3$		60.0	82.0	67.2	86.7	47.6	71.4	18.9	32.2	69.8	87.7
conv-medium	$3e-3$	54.5K	73.3	91.5	80.5	94.6	60.6	82.9	27.7	42.8	83.2	95.3
	$1e-3$		72.2	90.7	79.4	94.0	59.5	81.7	27.0	42.0	82.0	94.6
hybrid-medium	$3e-3$	44.3K	74.9	92.4	81.8	95.3	62.4	84.0	29.5	44.8	84.4	95.5
	$1e-3$		75.2	92.5	82.0	95.3	63.0	84.5	29.1	44.5	84.2	95.4

Table 8. SHViT results, obtained on 128×128 px images (%).

Size	Learning Rate	Throughput imgs/s	ImageNet-Val		ImageNet-ReaL		ImageNet-v2		ImageNet-R		ImageNet-HR	
			Top-1	Top-5	Top-1	Top-5	Top-1	Top-5	Top-1	Top-5	Top-1	Top-5
S1	$3e-3$	79.2K	63.5	84.9	70.9	89.1	50.8	74.5	22.2	35.7	73.7	90.0
	$1e-3$		63.5	85.1	71.0	89.3	50.9	74.4	21.3	34.7	72.9	90.5
S1	$3e-3$	75.1K	66.6	87.0	73.9	90.8	54.0	76.6	23.9	38.0	76.1	91.7
	$1e-3$		66.7	87.0	73.8	90.8	53.7	76.8	24.0	37.8	76.7	92.0
S3	$3e-3$	70.4K	70.5	89.8	77.7	93.1	58.1	80.4	26.6	41.0	80.4	93.8
	$1e-3$		71.2	90.0	78.3	93.3	58.6	80.7	26.7	40.7	80.7	93.9

Table 9. EfficientViT results, obtained on 128×128 px images (%).

Size	Learning Rate	Throughput imgs/s	ImageNet-Val		ImageNet-Real		ImageNet-v2		ImageNet-R		ImageNet-HR	
			Top-1	Top-5	Top-1	Top-5	Top-1	Top-5	Top-1	Top-5	Top-1	Top-5
B0	$3e-3$	98.6K	59.5	81.9	66.8	86.7	46.8	70.3	18.6	32.0	69.3	87.6
	$1e-3$		60.8	82.6	68.0	87.2	48.3	71.6	19.3	32.6	70.4	87.7
B1	$3e-3$	38.7K	71.8	90.7	79.2	94.0	59.7	81.8	27.4	42.2	81.5	94.4
	$1e-3$		72.8	91.0	79.8	94.2	60.4	81.9	27.1	42.3	82.5	94.8

Table 10. Finetuned results, obtained on 224×224 px images (%).

Architecture	Size	Throughput 224^2 px	ImageNet-Val		ImageNet-Real		ImageNet-v2		ImageNet-R		ImageNet-HR	
			Top-1	Top-5	Top-1	Top-5	Top-1	Top-5	Top-1	Top-5	Top-1	Top-5
ViT+Jumbo	$D=96, J=6$	43.1K	70.5	89.4	77.9	92.9	57.6	79.7	22.8	36.6	79.2	93.4
	$D=128, J=6$	31.9K	74.5	91.8	81.3	94.7	61.7	82.9	26.8	41.1	83.4	95.0
	$D=192, J=6$	19.9K	77.7	93.7	84.0	96.0	64.8	85.7	30.6	45.8	86.5	96.2
	$D=384, J=6$	7.8K	81.8	95.9	87.1	97.6	70.9	89.8	37.1	53.4	90.3	97.9
ViT+Registers	$D=128, R=16$	26.2K	61.0	84.1	68.9	88.9	49.1	74.1	18.7	32.4	69.7	88.9
	$D=192, R=16$	16.8K	74.5	92.3	82.3	95.4	62.5	84.7	28.2	43.5	83.7	95.6
	$D=384, R=16$	6.9K	81.9	96.0	87.4	97.7	71.4	90.2	38.0	53.8	90.0	98.0
MobileNetV4	conv-small	33.1K	65.6	86.2	73.3	90.7	52.5	75.5	22.3	37.5	75.7	91.3
	conv-medium	10.4K	74.9	92.6	82.4	95.5	63.1	84.8	29.4	45.9	84.7	95.8
	hybrid-medium	8.1K	78.1	94.3	85.0	96.7	67.0	87.5	33.0	49.4	87.2	96.8
SHViT	S1	40.9K	67.9	88.2	75.7	92.2	54.7	78.2	23.1	38.0	77.6	92.7
	S2	33.8K	71.0	90.0	78.6	93.6	58.4	80.5	25.6	41.1	80.9	93.9
	S3	23.1K	74.3	92.0	81.6	95.0	61.8	83.5	28.3	43.9	84.0	95.4
EfficientViT	B0	25.3K	66.3	86.5	73.9	90.7	53.6	76.3	22.2	36.7	75.8	91.0
	B1	9.6K	76.9	93.5	83.7	96.2	64.5	85.9	31.3	47.2	85.8	96.4

Table 11. Univariate time series classification results (%). “Best” refers to the best run of our 12-run hyperparameter sweep and “Avg” refers to the average over the sweep.

		PatchTST/8	PatchTST/8 +Registers	PatchTST/8 +Jumbo	PatchTST/42	PatchTST/42 +Registers	PatchTST/42 +Jumbo
Sleep	Best	70.9	70.7	73.3	70.5	70.6	70.3
	Avg	67.5	67.7	68.3	67.2	67.1	67.6
InsectSound	Best	82.8	83.3	83.7	85.8	84.4	85.6
	Avg	76.7	76.0	78.7	78.7	78.7	79.7
FruitFlies	Best	92.2	90.9	92.2	95.2	95.0	95.1
	Avg	88.4	88.4	89.4	93.1	92.9	93.9
RightWhaleCalls	Best	94.3	93.8	95.1	96.7	97.0	96.1
	Avg	92.8	93.5	94.2	94.0	94.8	95.1
FaultDetectionA	Best	98.0	97.7	98.1	99.6	99.8	99.8
	Avg	94.6	95.2	97.2	99.2	99.2	99.5
ElectricDevices	Best	89.0	88.8	90.1	92.4	92.4	92.5
	Avg	81.6	83.2	84.0	85.1	85.2	88.1
Crop	Best	80.9	81.2	82.0	81.2	80.6	82.2
	Avg	69.4	70.9	72.0	68.7	68.3	68.7
FordB	Best	98.8	97.3	97.7	97.7	96.5	96.5
	Avg	95.4	96.0	96.6	95.7	94.9	94.8
FordA	Best	97.3	98.0	97.7	97.1	97.1	97.5
	Avg	96.1	96.6	97.2	95.5	95.7	96.0
MelbournePedestrian	Best	92.1	91.5	91.0	90.4	91.0	93.1
	Avg	81.8	82.8	83.9	83.5	83.8	84.9

Table 12. Multivariate time series classification results (%). “Best” refers to the best run of our 12-run hyperparameter sweep and “Avg” refers to the average over the sweep.

		PatchTST/8	PatchTST/8 +Registers	PatchTST/8 +Jumbo	PatchTST/42	PatchTST/42 +Registers	PatchTST/42 +Jumbo
Tiselac	Best	96.6	96.9	97.2	96.4	96.4	96.7
	Avg	86.9	87.8	90.1	84.7	85.0	87.9
WalkingSittingStanding	Best	96.0	96.0	96.5	98.0	97.6	97.6
	Avg	91.7	89.8	93.5	93.9	93.9	94.5
SpokenArabicDigits	Best	99.9	99.7	99.9	99.7	99.9	99.9
	Avg	99.5	99.6	99.6	99.6	99.5	99.7
FaceDetection	Best	87.8	88.1	87.5	86.8	86.6	84.8
	Avg	78.9	80.9	80.0	77.4	77.4	78.8
PhonemeSpectra	Best	56.3	57.1	59.1	57.6	60.3	58.9
	Avg	38.2	38.7	46.5	42.9	44.5	47.7
LSST	Best	78.7	79.5	79.9	74.6	75.7	79.9
	Avg	69.3	69.4	71.2	61.4	61.4	67.3
UWaveGestureLibrary	Best	92.7	88.5	87.5	94.8	99.0	94.8
	Avg	76.8	79.9	83.4	81.3	83.5	85.4
CharacterTrajectories	Best	99.0	98.0	99.6	98.7	99.3	98.4
	Avg	93.6	94.2	96.6	96.6	95.2	97.0
AsphaltPavementTypeCoordinates	Best	72.3	77.7	81.1	89.5	88.5	89.5
	Avg	72.7	75.8	77.0	81.2	82.1	83.7
MotorImagery	Best	87.5	83.3	77.1	79.2	66.7	87.5
	Avg	84.9	83.3	83.2	73.6	74.0	81.9

